Diffusion Kurtosis Imaging Based on Adaptive Spherical Integral

Yugang Liu, Leiting Chen, and Yizhou Yu

***Abstract*—Diffusion kurtosis imaging (DKI) is a recent approach in medical engineering that has potential value for both neurological diseases and basic neuroscience research. In this letter, we develop a robust method based on adaptive spherical integral that can compute kurtosis based quantities more precisely and efficiently. Our method integrates spherical trigonometry with a recursive computational scheme to make numerical estimations in kurtosis imaging convergent. Our algorithm improves the efficiency of computing integral invariants based on reconstructed diffusion kurtosis tensors and makes DKI better prepared for further clinical applications.**

***Index Terms*—Adaptive spherical integral, kurtosis imaging, MRI, optimization.**

I. Introduction

DIFFUSION magnetic resonance imaging (MRI) is a medical imaging technique used in radiology to visualize microstructure of biological tissues. The MRI signal is attenuated by water diffusion in biological tissues. The amount of attenuation of diffusion-encoding gradient plus along one specific direction depends on the probability density function of projected displacements of water molecules along that gradient direction [1]. Thus, it becomes possible to reconstruct the full diffusion displacement probability density function for water molecules in the tissues. It is usually sufficient to characterize the diffusion characteristics with a scalar apparent diffusion coefficient (ADC) in *isotropic* matter. In *anisotropic* media, such as brain white matter, where the measured diffusivity is known to depend on the orientation of tissue, no single ADC can characterize the orientation-dependent water mobility in these tissues. Because of this, a zero-mean trivariate Gaussian function was proposed to model the diffusion tensor imaging (DTI), which reconstructs the full covariance tensor of the Gaussian function from multiple measurements.

A diffusion tensor D is a second-order three-dimensional positive semidefinite symmetric tensor [2], [3]. Under the Cartesian coordinate system, it is represented by a real three-dimensional symmetric matrix, with $D_{ij} = D_{ji}$ for $i, j = 1, 2, 3$. The MRI signal intensity $S_m(\mathbf{q})$ is expressed as follows in this model.

$$\ln[S_m(\mathbf{q})] = \ln[S_m(\mathbf{0})] - bD_{app}(\mathbf{x}) \tag{1}$$

where $\mathbf{q} = b\mathbf{x}$, $\mathbf{x}\left(=[x_1 \quad x_2 \quad x_3]^T\right)$ is a unit vector, $D_{app}(\mathbf{x})$ is the ADC value in the direction defined by $\mathbf{x}$

$$D_{app}(\mathbf{x}) = \sum_{i,j=1}^{3} D_{ij}\mathbf{x}_i\mathbf{x}_j \tag{2}$$

and the parameter b is given by

$$b = (\gamma\delta g)^2\left(\Delta - \frac{\delta}{3}\right) \tag{3}$$

where g is the gradient strength, γ is the proton gyromagnetic ratio, Δ is the separation time of the two diffusion gradients, and δ is the duration of each gradient lobe [4]. Combining (1) and (2), we have

$$\ln[S_m(\mathbf{q})] = \ln[S(0)] - b\sum_{i,j=1}^{3} D_{ij}\mathbf{x}_i\mathbf{x}_j. \tag{4}$$

DTI is known to have a limited capability in resolving water diffusion in the biologic tissues that is non-Gaussian. However, the complex structure of most tissues, consisting of various types of cells and membranes, can cause the diffusion displacement probability density function to deviate substantially from a Gaussian form. This deviation from Gaussian behavior can be quantified using a convenient dimensionless metric called the excess kurtosis. To estimate the excess kurtosis of water diffusion in vivo and describe the non-Gaussian behavior, the diffusion kurtosis imaging (DKI) has been proposed in [4]. A diffusion kurtosis tensor W is a fourth-order 3-D fully symmetric array, which has 15 independent elements $W = (W_{ijkl})$ with W_{ijkl} being invariant for any permutation of its indices i, j, k, l =1, 2, 3. Considering the diffusion kurtosis term, (1) can be expanded as follows:

$$\ln[S_m(\mathbf{q})] = \ln[S(0)] - bD_{app}(\mathbf{x}) + \frac{1}{6}b^2D_{app}^2(\mathbf{x})K_{app}(\mathbf{x}) \tag{5}$$

where $K_{app}(\mathbf{x})$ is the apparent kurtosis coefficient (AKC) value in the direction $\mathbf{x}$,

$$D_{app}^2K_{app} = \left(\frac{1}{3}\sum_{1}^{3} D_{ii}\right)^2 \sum_{i,j,k,l=1}^{3} W_{ijkl}\mathbf{x}_i\mathbf{x}_j\mathbf{x}_k\mathbf{x}_l. \tag{6}$$

Manuscript received December 04, 2010; revised January 25, 2011; accepted January 28, 2011. Date of publication February 10, 2011; date of current version February 17, 2011. This work was supported in part by National Science Foundation (IIS 09-14631) and China Scholarship Council. The associate editor coordinating the review of this manuscript and approving it for publication was Prof. Yong Man Ro.

Y. Liu and L. Chen are with the Department of Computer Science and Engineering, University of Electronic Science and Technology of China, Chengdu, 611731, China (e-mail: liulional@uestc.edu.cn).

Y. Yu is with Department of Computer Science, University of Illinois at Urbana-Champaign, Urbana, IL 61801 USA.

Color versions of one or more of the figures in this paper are available online at http://ieeexplore.ieee.org.

Digital Object Identifier 10.1109/LSP.2011.2113339

By combining (5), (2) and (6), we have

$$\ln[S_m(\mathbf{q})] = \ln[S(0)] - bD_{app} + \frac{1}{6}b^2\left(\frac{1}{3}\sum_{1}^{3}D_{ii}\right)^2 \sum_{i,j,k,l=1}^{3} W_{ijkl}\mathbf{x}_i\mathbf{x}_j\mathbf{x}_k\mathbf{x}_l. \quad (7)$$

Useful information related to tissue structure and patho-physiology may be contained in the non-Gaussian behavior of water molecules. Hence, diffusion kurtosis imaging (DKI) has important biological and clinical significance. Sharp differences between diffusion kurtosis values in white and gray matters have been illustrated in [4]. Techniques for kurtosis tensor reconstruction are introduced in [4]–[8]. Because clinical applications typically adopt invariant scalar quantities instead of originally reconstructed tensorial data, the D-eigenvalues method is proposed to analyze the diffusion kurtosis tensor and calculate the mean kurtosis and fractional kurtosis anisotropy, etc in [3], [9]. However, it is difficult to obtain accurate D-eigenvalues with methods in algebraic geometry [10]. In order to make diffusion kurtosis imaging more precise, our method based on adaptive spherical integral is proposed.

II. Methodology

First, a precondition for our method is that the diffusion tensor D and kurtosis tensor W have been reconstructed. To calculate kurtosis based quantities, we denote a unit sphere as S ($= \{\mathbf{x} \in \mathbb{R}^3 : x_1^2 + x_2^2 + x_3^2 = 1\}$). Then mean kurtosis is defined as follows:

$$M_K = \frac{1}{4\pi}\oiint_S K_{app}dA \quad (8)$$

where the AKC value K_{app} can be computed from (6), 4π is the area of surface S. Combining the definitions of kurtosis anisotropy in [3], [7], kurtosis anisotropy, K_A, is defined in this paper as follows:

$$K_A = \sqrt{\frac{\oiint_S (K_{app} - M_K)^2 dA}{\oiint_S K_{app}^2 dA}}. \quad (9)$$

It is easy to verify that $0 \le K_A \le 1$. If $K_A = 0$, the diffusion kurtosis tensor is isotropic. If $K_A = 1$, the diffusion kurtosis tensor is maximally anisotropic. In [9], mean kurtosis defined in (8) has proven to be an invariant. Similarly, since the directional distribution of K_{app} appearing in (5) is independent of any coordinate systems, its spherical integration is rotation invariant. Generally, mean kurtosis has relatively large values in regions with a relatively high fiber density and kurtosis anisotropy has relatively large values in regions filled with crossing fibers.

From the above definitions, we know the basic method of kurtosis imaging is dependent on integrals over the unit sphere S. To divide the domain of integration equally, we build a icosahedron inscribed in S, as shown in Fig. 1(a). In spherical trigonometry [11], the mappings between triangular faces of icosahedron and *spherical triangles* on S can be constructed. Consider three points A, B, and C on the surface of the sphere S in Fig. 1(b). If every two of them are connected by a great arc, we obtain a spherical triangle Π'. The angles of the spherical triangle Π', denoted by α, β, and γ, are angles between every two planes of the great circles. From Girard's Theorem, the area $A_{\Pi'}$ of spherical triangle Π' can be expressed by

$$A_{\Pi'} = r^2(\alpha + \beta + \gamma - \pi) \quad (10)$$

where r is the radius of sphere.

Algorithm 1 Recursive Subdivision of a Spherical Triangle

Declarations: Π' (spherical triangle), $A_{\Pi'}$ [the area of spherical triangle in (10)], S_t (standard deviation), θ (a threshold), $F_n(\mathbf{x})$ (integrand), i (=1, 2, 3, 4) (index).

procedure SUBDIVISION_SPHERICAL_TRIANGLE(Π', θ)

Divide the spherical triangle Π' into four subspherical triangles Π'_1, Π'_2, Π'_3, and Π'_4

$G_i \leftarrow$ center of subspherical triangle Π'_i

$\mathbf{x}_i \leftarrow$ unit direction of $\overrightarrow{OG'_i}$

$S_t \leftarrow$ standard deviation of $F_n(\mathbf{x}_i)$

if $S_t > \theta$ **then**

$I_s(\Pi') \leftarrow \sum_i$ SUBDIVISION_SPHERICAL_TRIANGLE(Π'_i, θ)

else

$I_s(\Pi') \leftarrow A_{\Pi'} \times$ the mean value of all items $F_n(\mathbf{x}_i)$

end if

end procedure

Result: $I_s(\Pi')$, integral of F_n over spherical triangle Π'.

To divide the unit sphere S into suitable sized spherical triangles for numerical integration, our adaptive spherical integral is based on two rules, "*reduction of variance*" and "*recursive stratified sampling*," in adaptive and recursive Monte Carlo methods [12]. Let Π' be a spherical triangle as in Fig. 1, D', E', and F' be the midpoints of the arcs $\widehat{AB}$, $\widehat{BC}$, and $\widehat{CA}$. Then we can obtain four subspherical triangles based on the points A, B, C, D', E', and F' as shown in Fig. 1(c)–(d). The center of each spherical triangle is the sample point for that triangle. For example, the center G_1 of the spherical triangle Π'_1 is the intersection between line OG'_1 and spherical triangle Π'_1, where O is the center of sphere S and G'_1 is the barycenter of triangle $\triangle AD'F'$. The steps of our recursive algorithm is illustrated in Algorithm 1. The integrand F_n in this algorithm can be chosen from (8) or (9).

Note that our numerical algorithm can reduce the approximation error by decreasing threshold θ. Recursive subdivision and sampling approximate the complex distribution of AKC values asymptotically. To indicate the convergence of our method, we use iterative reweighted model fitting [8] to reconstruct the diffusion tensor and kurtosis tensor for the white matter inside one volumetric pixel. The six independent elements of diffusion tensor D and 15 independent elements of kurtosis tensor W are

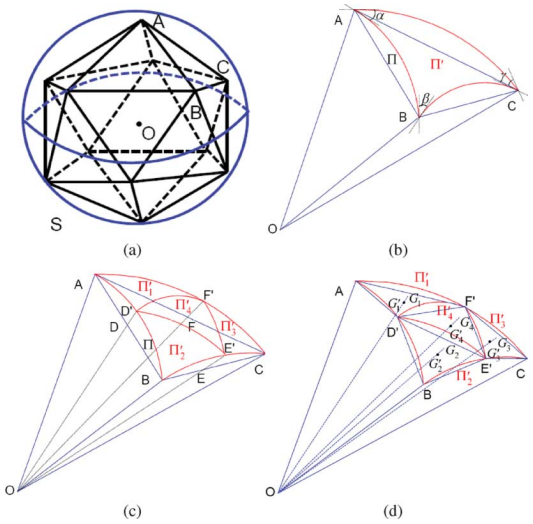

Fig. 1. Subdivision of spherical triangles. (a) An icosahedron inscribed in sphere S, (b) original spherical triangle Π', (c) spherical triangles (Π'_1, Π'_2, Π'_3, and Π'_4) after division, (d) centers of the spherical triangles.

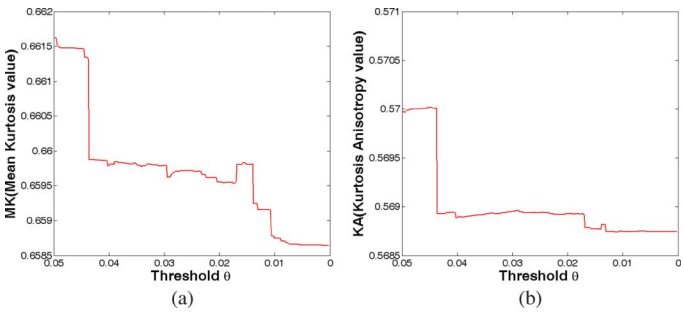

Fig. 2. Convergence of our algorithm by making threshold θ sufficiently close to 0. (a) Mean kurtosis and (b) Kurtosis anisotropy.

TABLE I
A RECONSTRUCTED DIFFUSION TENSOR D AND KURTOSIS TENSOR W IN WHITE MATTER

D_{11} 3.85×10^{-10}	W_{1111} 0.062	W_{2222} 1.300	W_{3333} 0.579
D_{22} 8.21×10^{-10}	W_{1112} −0.004	W_{1113} −0.079	W_{1222} 0.231
D_{33} 6.18×10^{-10}	W_{1333} 0.478	W_{2333} −0.028	W_{2223} −0.075
D_{12} 0.53×10^{-10}	W_{1122} 0.355	W_{1133} −0.059	W_{2233} 0.698
D_{13} 0.18×10^{-10}	W_{1123} −0.173	W_{1223} 0.034	W_{1233} 0.212
D_{23} -0.55×10^{-10}			

illustrated in Table I. The mean kurtosis and kurtosis anisotropy converge to stable values when the threshold θ become sufficiently small as shown in Fig. 2. Jumps caused by changes in spherical subdivision and sampling resolution become smaller as θ becomes smaller. Thus, important kurtosis based quantities can be obtained by adaptive spherical integral.

III. EXPERIMENTAL RESULTS

We have performed comparisons between our algorithm and D-eigenvalues based method in [3], [9]. D-eigenvalues based method computes eigenvalues of diffusion tensor D and kurtosis tensor W with techniques in algebraic geometry [10]. Kurtosis based quantities, such as mean kurtosis, can be obtained from these eigenvalues. However, these eigenvalues are apt to be affected by numerical errors. In addition, it is difficult to estimate

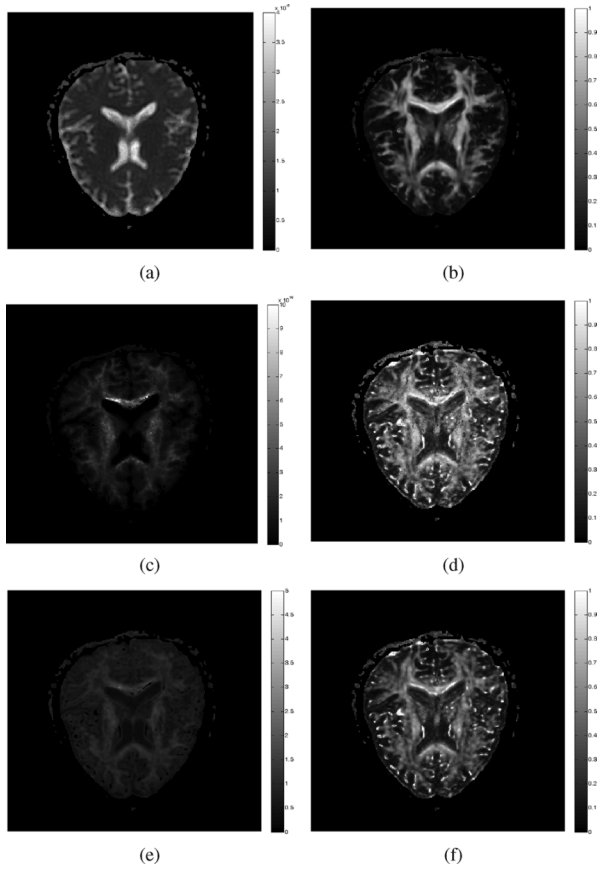

Fig. 3. Comparison of D-eigenvalues and adaptive spherical integral from 75 measurements. (a) Mean diffusivity, (b) fractional anisotropy, (c) mean kurtosis with D-eigenvalues, (d) fractional kurtosis anisotropy with D-eigenvalues, (e) mean kurtosis with adaptive spherical integral, and (f) kurtosis anisotropy with adaptive spherical integral.

error bounds for the numerical solutions as a small error in kurtosis tensor reconstruction may give rise to a much larger error in D-eigenvalues.

All the experiments have been implemented on an Intel Core 2 Duo 2.7 GHz processor with 2 GB memory. The measurements were collected with five levels of b values, which are 0, 500, 1000, 1500, 2000, and 2500, in unit of $\mathrm{s/mm^2}$, respectively. At each distinct b value except 0, 10 to 15 gradient directions were sampled over the unit sphere, resulting in 58 or 75 measurements per pixel. The parameters in (3) are proton gyromagnetic ratio $\gamma = 2.6751987 \times 10^8\ \mathrm{s^{-1}T^{-1}}$, separation time $\Delta = 0.038848$ s and duration of each gradient lobe $\delta = 0.0322$ s, respectively. The threshold θ in our algorithm is set to 0.001. To reconstruct the diffusion tensor D and kurtosis tensor W, the robust model fitting method in [8] is adopted in the model fitting stage.

To compare D-eigenvalues and adaptive spherical integral in kurtosis imaging, the same MRI data of a human brain was processed by both methods. The average processing time per pixel is 0.51 s with D-eigenvalues and 0.42 s with adaptive spherical integral, respectively. Fig. 3 shows kurtosis imaging results of a normal subject. The mean diffusivity (MD) and fractional anisotropy (FA) [2] are most common invariants in DTI. MD describes the relative degree of diffusion and FA describes the relative degree of anisotropy in diffusion tensor

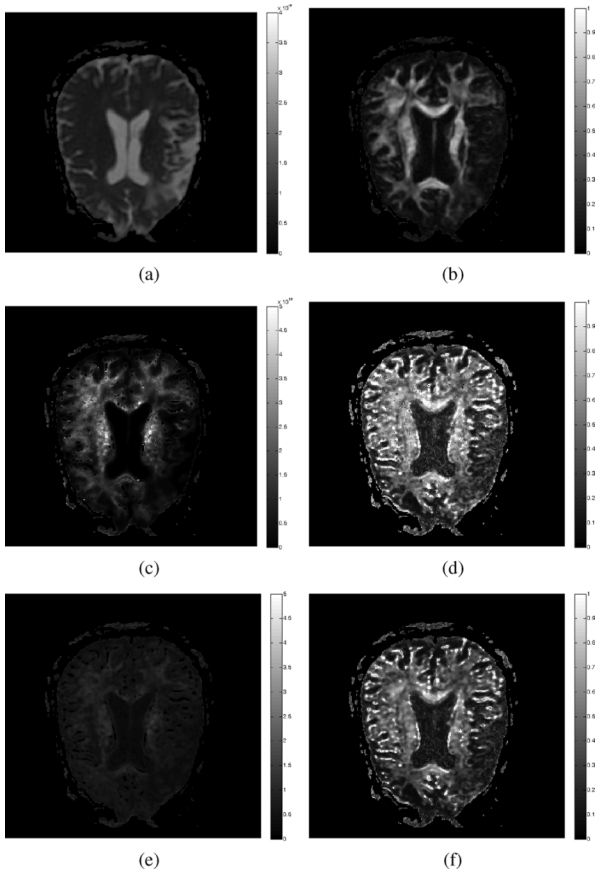

Fig. 4. Comparison of D-eigenvalues and adaptive spherical integral from 58 measurements. (a) Mean diffusivity, (b) fractional anisotropy, (c) mean kurtosis with D-eigenvalues, (d) fractional kurtosis anisotropy with D-eigenvalues, (e) mean kurtosis with adaptive spherical integral, and (f) kurtosis anisotropy with adaptive spherical integral.

TABLE II
A COMPARISON OF MEAN ERRORS AND NOISY POINT RATIOS. GROUND TRUTH DATA IS OBTAINED FROM 6860 SUB-TRIANGLES ON THE SPHERE AND ADAPTIVE SPHERICAL INTEGRAL USUALLY NEEDS 400-800 SUB-TRIANGLES. IF THE MINIMUM ABSOLUTE DIFFERENCE WITH ITS FOUR IMMEDIATE NEIGHBORS IS LARGER THAN 0.4, WE CLASSIFY IT AS A NOISY PIXEL. (KAD: FRACTIONAL KURTOSIS ANISOTROPY WITH D-EIGENVALUES, KAA: KURTOSIS ANISOTROPY WITH ADAPTIVE SPHERICAL INTEGRAL)

Experiment	Mean Error		Noisy Point Ratio	
	KAD	KAA	KAD	KAA
Fig. 3	0.0087	0.0005	0.061%	0.017%
Fig. 4	0.0336	0.0006	0.077%	0.051%

D. Since the range of KA is the same as FA, the values in Fig. 3(b), (d), and (f) are within interval $[0, 1]$. Non-Gaussian information can be observed in kurtosis images, but not in the FA image. In Fig. 3(d) and (f), it is easy to verify that there exist more noisy dots in the results based on D-eigenvalues. Similarly, more noisy dots appear in MK images estimated using D-eigenvalues, such as in Figs. 3(c) and 4(c). To analyze their numerical performance, we compute the mean error against ground truth for each method and also its ratio of noisy pixels as shown in Table II. The ground true is estimated using an overly subdivided sphere. Our numerical integration with adaptive subdivision clearly outperforms the method based on D-eigenvalues.

Fig. 4 shows kurtosis imaging results of a stroke patient. The asymmetry between the left cerebral hemisphere and right cerebral hemisphere can be easily observed in FA and KA results. As in the previous experiment, more clinical information can be obtained from kurtosis based quantities. The image of kurtosis anisotropy with adaptive spherical integral is also cleaner than the results with D-eigenvalues according to Fig. 4(d) and (f).

IV. CONCLUSIONS

We have presented a convergent method for computing kurtosis based invariant quantities using adaptive spherical integral. A new definition of kurtosis anisotropy (9) has been proposed. And our algorithm estimates kurtosis based quantities more accurately and efficiently in the experiments performed on clinical data.

ACKNOWLEDGMENT

The authors wish to thank S. Wei at Zhejiang University for providing the Matlab code for computing D-eigenvalues.

REFERENCES

[1] D. C. Alexander, "Multiple-fiber reconstruction algorithms for diffusion mri," *Ann. New York Acad. Sci.*, vol. 1064, pp. 113–133, 2005.
[2] D. L. Bihan, J.-F. Mangin, C. Poupon, C. A. Clark, S. Pappata, N. Molko, and H. Chabriat, "Diffusion tensor imaging: Concepts and applications," *J. Magn. Res. Imag.*, vol. 13, no. 4, pp. 534–546, Apr. 2001.
[3] L. Qi, Y. Wang, and E. X. Wu, "D-eigenvalues of diffusion kurtosis tensors," *J. Comput. Appl. Math.*, vol. 221, no. 1, pp. 150–157, Nov. 2008.
[4] J. H. Jensen, J. A. Helpern, A. Ramani, H. Lu, and K. Kaczynski, "Diffusional kurtosis imaging: The quantification of non-Gaussian water diffusion by means of magnetic resonance imaging," *J. Magn. Res. Imag.*, vol. 53, no. 6, pp. 1432–1440, Jun. 2005.
[5] M. Lazar, J. H. Jensen, L. Xuan, and J. A. Helpern, "Estimation of the orientation distribution function from diffusional kurtosis imaging," *Magn. Res. Med.*, vol. 60, no. 4, pp. 774–781, Oct. 2008.
[6] J. Veraart, D. H. J. Poot, W. V. Hecke, I. Blockx, A. V. der Linden, M. Verhoye, and J. Sijbers, "More accurate estimation of diffusion tensor parameters using diffusion kurtosis imaging," *Magn. Res. Med.*, vol. 65, no. 1, pp. 138–145, Jan. 2011.
[7] D. H. J. Poot, A. J. den Dekker, E. Achten, M. Verhoyed, and J. Sijbers, "Optimal experimental design for diffusion kurtosis imaging," *IEEE Trans. Med. Imag.*, vol. 29, pp. 819–829, Mar. 2010.
[8] Y. Liu, S. Wei, Q. Jiang, and Y. Yu, "Reconstructing diffusion kurtosis tensors from sparse noisy measurements," in *Proc. IEEE Int. Conf. Image Processing*, Sep. 2010, pp. 4185–4188.
[9] L. Qi, D. Han, and E. X. Wu, "Principal invariants and inherent parameters of diffusion kurtosis tensors," *J. Math. Anal. Applicat.*, vol. 349, no. 1, pp. 165–180, Jan. 2009.
[10] D. A. Cox, J. B. Little, and D. O'Shea, *Using Algebraic Geometry*, 1st ed. Berlin, Germany: Springer, 1998.
[11] I. N. Bronshtein, K. A. Semendyayev, G. Musiol, and H. Muehlig, *Handbook of Mathematics*, 5th ed. Berlin, Germany: Springer-Verlag, 2007.
[12] W. H. Press, S. A. Teukolsky, W. T. Vetterling, and B. P. Flannery, *Numerical Recipes in C: The Art of Scientific Computing*, 2nd ed. New York: Cambridge Univ. Press, 1992.